
Article:
Alix, J.J.P. orcid.org/0000-0001-8391-9749, Plesia, M., Lloyd, G.R. et al. (7 more authors) (2022) The application of Raman spectroscopy to the diagnosis of mitochondrial muscle disease : a preliminary comparison between fibre optic probe and microscope formats. Journal of Raman Spectroscopy, 53 (2). pp. 172-181. ISSN 0377-0486

https://doi.org/10.1002/jrs.6273

The application of Raman spectroscopy to the diagnosis of mitochondrial muscle disease: a preliminary comparison between fibre optic probe and microscope formats

Journal:	*Journal of Raman Spectroscopy*
Manuscript ID	JRS-21-0154.R2
Wiley - Manuscript type:	Research Article
Date Submitted by the Author:	06-Oct-2021
Complete List of Authors:	Alix, James; The University of Sheffield, Sheffield Institute for Translational Neuroscience Plesia, Maria; Sheffield Institute for Translational Neuroscience Lloyd, Gavin; Phenome Centre Dudgeon, Alex; School of Physics and Astronomy Kendall, Catherine; Biophotonics Research Unit McDermott, Christopher; Sheffield Institute for Translational Neuroscience Gorman, Grainne; NHS Highly Specialised Service for Rare Mitochondrial Disorders Taylor, Robert; NHS Highly Specialised Service for Rare Mitochondrial Disorders Shaw, Pamela; Sheffield Institute for Translational Neuroscience Day, John; School of Physics
Keywords:	Raman spectroscopy, biomedical, neurology, Mitochondrial disease, Diagnosis

The application of Raman spectroscopy to the diagnosis of mitochondrial muscle disease: a preliminary comparison between fibre optic probe and microscope formats

James J.P. Alix[1,2 *], Maria Plesia[1], Gavin R. Lloyd[3], Alexander P. Dudgeon[4,5], Catherine A. Kendall[4], Christopher J. McDermott[1,2], Gráinne S. Gorman[6,7], Robert W. Taylor[6,7], Pamela J. Shaw[1,2], John C. Day[8]

[1]Sheffield Institute for Translational Neuroscience, University of Sheffield

[2]Neuroscience Institute, University of Sheffield

[3]Phenome Centre, University of Birmingham

[4]Biophotonics Research Unit, Gloucestershire Hospitals NHS Foundation Trust

[5]Biomedical Spectroscopy, School of Physics and Astronomy, University of Exeter

[6]Wellcome Centre for Mitochondrial Research, Translational and Clinical Research Institute, Faculty of Medical Sciences, Newcastle University, Newcastle upon Tyne

[7]NHS Highly Specialised Service for Rare Mitochondrial Disorders, Newcastle upon Tyne Hospitals NHS Foundation Trust, Newcastle upon Tyne, UK

[8]Interface Analysis Centre, School of Physics, University of Bristol

***Correspondence**

Dr James J.P. Alix

Sheffield Institute for Translational Neuroscience, 385a Glossop Road, Sheffield, S10 1HQ, UK.

Email: j.alix@sheffield.ac.uk

Telephone: 0114 215 9100

Key words: Raman spectroscopy; biomedical; neurology; mitochondrial disease; diagnosis

Abstract

Muscle biopsy remains an important component of the diagnostic repertoire for patients with suspected mitochondrial disease, underpinning specialist histopathological and biochemical analyses. Raman spectroscopy has not yet been applied to mitochondrial disease and new fibre optic systems, with advantages in terms of cost and portability, could provide a rapid means to identify muscle pathology. In this study, we aimed to explore the potential of two different formats of Raman spectroscopy to identify mitochondrial disease: a miniaturised fibre optic Raman system and a standard commercial Raman microscope. Raman spectra were recorded from muscle samples from healthy volunteers (n=10) and patients with genetically confirmed mitochondrial disease (n=15). Multivariate classification algorithms demonstrated a high level of disease classification performance with both the fibre optic probe system and microscope (area under receiver operating characteristic curves 0.80 – 0.82). Key spectral changes associated with mitochondrial disease concerned relating to the α-helical configuration of proteins. The results suggest that Raman spectroscopy of muscle is worthy of further investigation as a technique for the rapid identification of mitochondrial disease.

Keywords

Raman spectroscopy, muscle, mitochondrial disease, fibre optic

Introduction

Mitochondrial are cytoplasmic organelles that synthesise adenosine triphosphate (ATP), the energy currency of cells. However, these organelles also play a role in a range of other metabolic pathways; as a result, disorders of mitochondrial function are an extraordinarily complex group of genetic conditions. They are among the most common inherited metabolic disorders with a prevalence in children of 5-15 cases per 100,000[1] and approximately 20 per 100,000 in adults.[2] A wide range of clinical symptoms can be observed arising from any organ or tissue, often involving multiple systems such as, the nervous, cardiovascular and endocrine systems.[3]

Muscle weakness due to muscle dysfunction and atrophy, known as myopathy, is a common neurological feature seen in mitochondrial disease. However, patients usually also manifest a range of other neurological symptoms, for example, poor balance (ataxia), hearing loss and epilepsy, as well as evidence of dysfunction in a range of other body systems. The wide range of clinical presentations encountered makes both diagnosis and management extremely challenging. The so-called "mitochondrial diagnostic odyssey"[4] is further complicated by the wide range of genetic abnormalities encountered, with over 350 disease genes across the nuclear and mitochondrial genomes associated with mitochondrial disease.[5]

Genetic analyses, in particular gene agnostic, next-generation sequencing strategies, are leading to a step-change in the understanding of mitochondrial disease and now represent the diagnostic gold standard. However, analysis of muscle tissue obtained from a muscle biopsy can be an important part of the diagnostic work up. In the complicated diagnostic landscape of

mitochondrial disease, a simple test to identify mitochondrial disorders would facilitate diagnosis and referral to the small number of specialist centres that manage these patients.

Raman spectroscopy is a rapid means to assess the biochemical composition of tissue. The technique is based upon the inelastic scattering of light, with the energy shift of the scattered light caused by the vibrational modes of different molecules within the tissue. Standard laboratory formats are microscope-based, but fibre optic methods are rapidly gaining attention as technological advances have improved the collection of the weak Raman signal.[8] Fibre optic formats have several advantages including cost, portability and the potential for *in vivo* measurements in clinical environments.

Biomedical Raman spectroscopy gained early momentum in the identification of different cancers[9]. Recently the technique has been used to investigate blood samples from several neurological disorders including dementia[10], multiple sclerosis[11] and amyotrophic lateral sclerosis.[12] Raman spectroscopy has also proved capable of identifying muscle abnormalities in the context of disuse atrophy[13], ischaemia, myopathy[14] and motor neurone disease.[15] With no need for tissue preparation, Raman spectroscopy is thus an interesting methodology to assess in the context of neurological disorders which can prove difficult to diagnose.

In the present study we have used *ex vivo* human muscle samples to explore the potential of Raman spectroscopy of muscle to identify mitochondrial disorders prior to any sample preparation. As a fibre optic probe could potentially be used to take *in vivo* human measures we have tested two different technologies for the acquisition of Raman data, a standard commercial microscope and a miniaturised fibre optic probe.[16]

Methods

Participants

A total of 25 participants were included with each participant contributing a single muscle biopsy sample. Samples from patients with mitochondrial disease were collected through conchotome needle biopsy technique and snap frozen in Newcastle, in accordance with standard operating procedures for the histopathological processing of human muscle samples. Each sample comprised >300 muscle fibres when cryosectioned in transverse orientation, an appropriate number of fibres for diagnostic histopathological studies. Healthy volunteer samples were collected at the time of knee surgery (anterior cruciate ligament repair) from muscles exposed during the operation. The use of human tissue was approved by the Newcastle and North Tyneside Local Research Ethics Committees (reference 09/H0906/75), with samples excess to diagnosis stored within the Newcastle Mitochondrial Research Biobank (REC reference: 16/NE/0267).

The demographic and clinical characteristics of the participants is given in Table 1. Further clinical and histological details can be found in Table S1 (Supporting Information).

Raman spectroscopy

An in-house miniature (0.5 mm) fibre optic Raman probe was housed within a standard 21-guage hypodermic needle[16]; Fig. S1 (Supporting Information). The probe optics consisted of two identical short lengths (<15cm) of low-OH, 105μm core fibre (Thor Labs Inc) contained in a single cannula. One fibre constituted the excitation path and the other the signal collection path. Each probe fibre was connected via an inline filter unit to a low-OH fibre patch-cord and then to the laser or spectrometer as appropriate. A laser bandpass filter (Semrock inc) was used

in the excitation arm to reject inelastically scattered light generated in the delivery patch-cord. An 830nm long wavelength pass filter (Semrock inc) was used in the collection arm to prevent elastically scattered light from the sample returning to the detection system. A fibre-coupled 830 nm semiconductor laser (Innovative Photonics Solutions) was used with a power of 60mW at the probe tip. A~~, which a~~lthough 830nm excitation may result~~ing~~ in a lower total signal than shorter wavelength excitation, it may provide a superior signal-to-noise ratio due to lower background fluorescence and does not cause photodamage.[17] ~~A laser line bandpass filter (Semrock Inc.) was used to remove Raman and fluorescence generated within the delivery fibre. This filtered light was refocused into a short length (<15 cm) of low-OH fibre (Thor labs, Inc.). An identical second fibre was used to collect scattered light, and relay to the spectrometer via an inline filter unit containing a long pass filter to reject elastically scattered light. The probe provided a recording volume of ~0.25mm^3.~~ To optimise detection efficiency, a spectrometer with numerical aperture matching that of the fibre was used ~~This fibre was optically matched to the spectrometer~~ (Raman Explorer Spectrograph, Headwall Photonics, Inc. and iDus 420BR-DD CCD camera, Andor Technology, Ltd.). In addition, the fibre core was used as the defining entrance aperture to the spectrometer, obviating the need for an entrance slit. ~~for optimum efficiency.~~ Samples were stored at -80˚C and allowed to thaw to room temperature prior to measurements. A robust Raman signal of interest was recorded through a 40-second exposure consisting of four 10 second epochs which were averaged. The probe collected signal from a sample volume of ~0.25mm^3.

Raman spectra were also collected using a microscope (x50 objective, 830nm excitation laser, 30mW power at the objective) coupled with a Renishaw Raman spectrometer system (System 1000, Renishaw Plc.). Muscle samples were placed on a calcium fluoride slide and spectra

were first obtained using the fibre optic probe. The slide was then transferred to the microscope for further data collection. Spectra from both the fibre optic and microscope systems were collected from 2-6 sites from each sample, depending upon sample size. Acquisition time at each site was 40s.

Analysis

Analysis was done in MATLAB (MATLAB R2019b The MathWorks, Inc., Natick, MA). Spectra collected by the fibre optic probe were first windowed between 900 – 1800 cm^{-1} as outside this region the spectra were dominated by peaks and background related to the silica in the optical fibres (< 900 cm^{-1}) or consisted of uninformative noise (> 1700 cm^{-1}). Microscope spectra presented in the main text were windowed between 600 – 1700 cm^{-1}; analyses were also repeated with windowing similar to the fibre optic system (900 – 1700 cm^{-1}, Fig. S2 (Supporting Information)). Windowed raw spectra were pre-processed in a similar fashion to other studies of human tissue with interpolation to integer wavenumber spacings, standard normal variate normalisation (SNV) and smoothing (2nd order Savitzky–Golay filter, 7 data point window width[18]). Spectral background was removed using the adaptive, iteratively reweighted penalized least squares (airPLS) algorithm.[19] Difference spectra were taken without background subtraction.

For multivariate analysis, spectra were mean centred prior to principal component analysis followed by linear discriminant analysis (PCA-LDA), or partial least squares discriminant analysis (PLS-DA). For PCA-LDA, t-tests were performed on the first 10 PCs with false discovery rate correction (Q=0.05) and significant PCs selected input to the LDA. Linear discriminant functions (LDF) plots were constructed and used to illustrate the peaks

contributing most to the discrimination between healthy and diseased tissue. Nested t-tests of linear discriminant function scores (spectra nested within participants) were undertaken using GraphPad Prism (version 9). Multivariate analysis of variance was undertaken using JASP (version 0.14.1).[20] For analyses on the proportion of cytochrome c oxidase(COX)-deficient fibres, samples were grouped as having a low proportion of/no COX-deficient fibres (<5%[21]), or a ~~higher~~ high proportion of COX-deficient fibres (≥5%, although in this cohort all such patients had >15%). For PLS-DA the number of latent variables included in the classification models was increased incrementally until the ability of the algorithm to accurately predict test set spectra no longer increased. Classification was undertaken utilising leave-one-patient-out cross validation to avoid overfitting. Sensitivity, specificity, accuracy and area under the receiver operator characteristic curve (AUROC) were calculated. Partial least squares regression was performed using the PLS_Toolbox (Eigenvector Research Inc.) to assess for correlation between age and the spectra.

Results

Raman spectral analysis

Raman spectra were recorded using both the fibre optic probe and microscope systems (Fig. 1). The spectra comprised peaks previously documented in a variety of skeletal muscle preparations,[22-24] as well as Raman peak assessments of muscle components such as myosin,[25] actin[26] and collagen.[27] Tentative peak assignments are shown in Table S2 (Supporting Information). Difference spectra from both modalities, reflecting the molecular/biochemical changes associated with disease, demonstrated consistent reductions at 1445-50 cm^{-1} relating to collagen and phospholipids, as well as at 1300 cm^{-1} and 1655 cm^{-1}, relating to the α-helical configuration of proteins.

The healthy volunteer muscle sampled was exclusively from the gracilis/semitendinous muscles, whereas in the mitochondrial disease patients, a range of muscles were biopsied (Table 1). While differences between muscles exist, for example, in fibre type composition, these overlap considerably. To investigate the potential effect of different muscle types, healthy tissue spectra were subtracted from those obtained from two different patient muscles (quadriceps and tibialis anterior). These demonstrated similar difference peaks (Fig. 2). By contrast, subtraction spectra of the two mitochondrial muscles were quite different, suggesting that the disease/healthy differences were underpinned by different spectral features to those determining muscle differences. In addition, while muscle can manifest age-related changes, in the mitochondrial disease patients the underling pathology would be expected to dominate.[6] Using PLS-R, no clear correlation between age and muscle spectra was observed (for the probe:

R^2 = 0.219 and root mean square error of cross validation (RMSECV) = 15.7; for the microscope: R^2 = 0.29 RMSECV = 15.7; Fig. S2 (Supporting Information)).

Multivariate analysis

Despite the presence of disease, the muscle tissues from the mitochondrial disease will retain many common biochemical features with healthy muscle tissue, as can be seen from the averaged and difference spectra. We therefore performed multivariate analyses to further assess differences between the two groups. These demonstrated significant differences in the LDF scores between the mitochondrial disease patients and healthy volunteers for both the probe and microscope formats (Fig. 3). The respective loadings plots demonstrated peaks common with the subtraction spectra, as well as new information. Classification performance was comparable for both the fibre optic probe and microscope systems (Table 2). Repeating the analyses with the microscope data windowed to the same spectral range as the fibre optic probe did not alter the LD loadings plot (Fig. S3, Supporting Information) and classification performance statistics were unchanged (not shown).

In the histopathological analysis of muscle specimens, the proportion of muscle fibres deficient in COX activity, an essential enzyme of mitochondrial oxidative phosphorylation, is typically assessed. Unsupervised PCA revealed clusters of patients (based on the proportion of COX-deficient fibres) and healthy volunteers, with PCA-LDA and PLS-DA both demonstrating accurate identification of samples within three group models (Fig. 4).

Discussion

Our results show that spontaneous Raman spectroscopy of muscle specimens is a promising technique for the identification of mitochondrial disease in *ex vivo* muscle specimens. Given the clinical and genetic heterogeneity of mitochondrial disease and the difficulties in achieving a diagnosis, the development of simple, rapid tests to guide the diagnostic process is an important challenge. Our work represents a first step towards the utilisation of Raman spectroscopy in the diagnosis of this devastating group of conditions. Interestingly, both the microscope and fibre optic formats were able to discriminate between healthy and patient groups.

The Raman data appear to contain a number of peaks with potential relevance to muscle pathology. Both subtraction and multivariate analyses from both the microscope and fibre optic probe systems shared common peaks, relating to α-helical protein content e.g. both formats demonstrated a relative loss of intensity in disease at 1250-1350 cm^{-1} and 1655 cm^{-1}).[28] Work in preclinical models of human neuromuscular diseases from both our group and others have demonstrated similar changes in muscle, suggesting a relative loss of such structures in disease states.[14] Alterations in lipid related peaks (e.g. 1080/1086 cm^{-1}) were also observed and perhaps relate to the important role of mitochondria in lipid metabolism.[29]

We obtained comparable results from the microscope and fibre optic probe measurements, although these two methods inevitably produce some differences in spectra. The mean spectra from both formats share common prominent peaks but also manifest differences in the spectral shape (e.g. between 1250-1350 cm^{-1}; Fig. 1). Similarly, there are common peaks in the patient vs. healthy volunteer difference spectra (Fig.2). The difference spectra taken between muscles

from patients with mitochondrial disease show greater discrepancies, although differentiating between biological signal and background noise in the low intensity probe spectrum (Fig. 2e) is difficult. Similarly, the microscope difference spectrum between mitochondrial disease muscles (Fig. 2f) also suffers from less clear biological information. Thus, when the biological differences between samples is limited the two formats appear to show greater variation. One can only speculate as to the exact reasons for this. The fibre optic probe samples a considerably larger volume which increases the likelihood of including the target pathologies. However, this configuration does give a higher artificial background due to the contributions from the silica fibre optic core. The fibre optic system also has a lower resolution than the microscope, which could cause peaks to wide and, potentially, merge. Differences between the probe and microscope may also stem from the higher power density produced by the microscope objective, which is more likely to cause photobleaching of any fluorescent background. Some differences may also be attributed to etaloning in the back thinned CCD detector used on the fibre optic probe spectrometer.

While we endeavoured to collect fibre optic and microscope data from similar areas of the biopsy, it is unlikely that the same area of muscle was sampled with both techniques. Spectra obtained using both the probe and microscope were more variable in the patient group, as can be appreciated by the wider standard deviation in figure 1. This is likely to be due to there being some areas of muscle in the patient group that are more affected by pathological changes than others. As we have not targeted histopathologically defined areas of abnormality it is inevitable that we will have collected data from areas with differing molecular changes. Notwithstanding all these challenges, these data suggest that Raman spectroscopy is sensitive to the biochemical changes associated with mitochondrial muscle pathology. An optical biopsy using fibre optic

technology may therefore be feasible in humans, as we have shown in mice.[15] A rapid, simple to use test, capable of identifying disease at the bedside in human patients, and at the bench in preclinical models, would augment not only the diagnostic pathway for patients with complex mitochondrial disease, but also the pull-through of preclinical research into clinical trials.

The major challenges for this preliminary study relate to differences in the age and muscle biopsied of the patient and healthy volunteer groups. Such differences are not uncommon in studies exploring the biomedical applications of vibrational spectroscopy with human biosamples.[10] Our data suggest that differences in age were not driving the classification observed between patient and healthy volunteer muscle, although clearly much larger studies would be needed to prove this unequivocally. Similarly, different muscles were sampled in the two patient groups. While different muscles can have specific histological features, such as differences in fibre type composition and fibre size, in the muscles sampled in this study these will overlap.[30-31] Notwithstanding these challenges, our analysis suggests disease-related spectral features can be found with spontaneous Raman spectroscopy. More detailed studies, for example, sample mapping approaches, may reveal additional features, such as variation in mitochondrial pathology at the single muscle fibre level.[6] The use of techniques such as resonance Raman spectroscopy aimed, for example, at assessing COX activity might provide a useful readout of disease state.

In addition, we only had a small number of samples for each patient group which affect sensitivity/specificity estimates through over-fitting. To reduce this, we limited the number of principal components assessed (max. of 10), and then utilised only those components with statistically significant differences between the patient/healthy volunteer groups. In addition,

unlike several other studies of pathological specimens, we have not histologically analysed the samples in the discrete areas that have undergone Raman measurement.[32-33] Our aim was to assess the potential of the technique to rapidly identify muscle pathology, prior any sample preparation. Thus, targeting the signal/analysis to a histopathologically defined area would likely increase classification model performance.

In the "genetics first" diagnostic landscape of mitochondrial disease it is useful to consider the potential role of Raman spectroscopy of muscle in the clinic. While genetic studies are usually undertaken in non-invasively obtained tissues (e.g. EDTA blood, urinary sediments) skeletal muscle is still studied as a clinically-relevant tissue and useful post-mitotic surrogate for other commonly affected organs, such as brain and the central nervous system. The relative simplicity of spontaneous Raman spectroscopy may also prove useful way in screening for mitochondrial dysfunction in the context of genetic variants of unknown significance, stratifying patients with pathogenic mutations, or when mitochondrial disease had not been clinically suspected. Furthermore, the performance of the fibre optic system raises the possibility of real-time bedside testing for mitochondrial dysfunction, without the need for a more invasive biopsy.

In this study we used spontaneous Raman which provides a relatively weak signal. Alternative approaches are available, such as surface-enhanced Raman spectroscopy (SERS[34]), or coherent anti-Stokes Raman scattering (CARS).[35] Each of these have their own technical difficulties/limitations (e.g. consistency in the fabrication of substrates for SERS; collection of information at one Raman wavenumber in traditional CARS). While solutions are emerging, each solution increases the complexity of the arrangement and associated cost. Our approach

represents arguably the simplest possible arrangement for the collection of Raman data and the most practical for *in vivo* clinical diagnostics.

Conclusions

In summary, we have assessed the potential utility of Raman spectroscopy for the rapid identification of muscle pathology caused by mitochondrial disease. Using a fibre optic Raman probe and a commercial Raman microscope we observed an accurate classification of muscle samples from patients with genetically-confirmed mitochondrial disease and healthy volunteers. Despite several limitations, our results demonstrate the feasibility of Raman spectroscopy as a rapid, simple, label free technique for studying muscle in the context of mitochondrial disease. The comparable performance of fibre optic and microscope formats highlights potential of fibre optic technology in evaluating muscle pathology.

Funding

The work was funded by an Academy of Medical Sciences Starter grant (SGL015\1001; JJPA, PJS, JCCD). PJS is supported as a National Institute for Health Research (NIHR) Senior Investigator (NF-SI-0617–10077) and by the NIHR Sheffield Biomedical Research Centre (IS-BRC-1215-20017). RWT is supported by the Wellcome Centre for Mitochondrial Research (203105/Z/16/Z), the Medical Research Council (MRC) International Centre for Genomic Medicine in Neuromuscular Disease (MR/S005021/1), the Mitochondrial Disease Patient Cohort (UK) (G0800674), the Lily Foundation, the Pathology Society and the UK NHS Specialised Commissioners who fund the "Rare Mitochondrial Disorders of Adults and Children" Service in Newcastle upon Tyne.

References

[1] D. Skladal, J. Halliday and D. R. Thorburn, *Brain* **2003**, *126*, 1905.
[2] G. S. Gorman, A. M. Schaefer, Y. Ng, N. Gomez, E. L. Blakely, C. L. Alston, C. Feeney, R. Horvath, P. Yu-Wai-Man, P. F. Chinnery, R. W. Taylor, D. M. Turnbull and R. McFarland, *Ann Neurol* **2015**, *77*, 753.
[3] G. S. Gorman, P. F. Chinnery, S. DiMauro, M. Hirano, Y. Koga, R. McFarland, A. Suomalainen, D. R. Thorburn, M. Zeviani and D. M. Turnbull, *Nat Rev Dis Primers* **2016**, *2*, 16080.
[4] J. Grier, M. Hirano, A. Karaa, E. Shepard and J. L. P. Thompson, *Neurol Genet* **2018**, *4*, e230.
[5] S. L. Stenton and H. Prokisch, *Essays Biochem* **2018**, *62*, 399.
[6] C. L. Alston, M. C. Rocha, N. Z. Lax, D. M. Turnbull and R. W. Taylor, *J Pathol* **2017**, *241*, 236.
[7] S. T. Ahmed, L. Craven, O. M. Russell, D. M. Turnbull and A. E. Vincent, *Neurotherapeutics* **2018**, *15*, 943.
[8] O. Stevens, I. E. Iping Petterson, J. C. Day and N. Stone, *Chem Soc Rev* **2016**, *45*, 1919.
[9] A. C. S. Talari, Z. Movasaghi, S. Rehman and I. u. Rehman, *Applied Spectroscopy Reviews* **2015**, *50*, 46.
[10] M. Paraskevaidi, C. L. M. Morais, D. E. Halliwell, D. M. A. Mann, D. Allsop, P. L. Martin-Hirsch and F. L. Martin, *ACS Chem Neurosci* **2018**, *9*, 2786.
[11] S. Alba-Arbalat, M. Andorra, B. Sanchez-Dalmau, A. Camos-Carreras, M. Dotti-Boada, I. Pulido-Valdeolivas, S. Llufriu, Y. Blanco, M. Sepulveda, A. Saiz, O. Batet, I. Bilbao, I. Torre, I. Amat-Roldan, E. H. Martinez-Lapiscina and P. Villoslada, *Invest Ophthalmol Vis Sci* **2021**, *62*, 11.
[12] C. F. Morasso, D. Sproviero, M. C. Mimmi, M. Giannini, S. Gagliardi, R. Vanna, L. Diamanti, S. Bernuzzi, F. Piccotti, M. Truffi, O. Pansarasa, F. Corsi and C. Cereda, *Nanomedicine* **2020**, *29*, 102249.
[13] M. Azeem, R. Qaisar, A. Karim, A. Ranade and A. Elmoselhi, *Biochem Biophys Rep* **2021**, *25*, 100930.
[14] R. Gautam, S. Vanga, A. Madan, N. Gayathri, U. Nongthomba and S. Umapathy, *Anal Chem* **2015**, *87*, 2187.
[15] M. Plesia, O. A. Stevens, G. R. Lloyd, C. A. Kendall, I. Coldicott, A. J. Kennerley, G. Miller, P. J. Shaw, R. J. Mead, J. C. C. Day and J. J. P. Alix, *ACS Chem Neurosci* **2021**, *12*, 1768.
[16] J. C. Day and N. Stone, *Appl Spectrosc* **2013**, *67*, 349.
[17] H. J. Butler, L. Ashton, B. Bird, G. Cinque, K. Curtis, J. Dorney, K. Esmonde-White, N. J. Fullwood, B. Gardner, P. L. Martin-Hirsch, M. J. Walsh, M. R. McAinsh, N. Stone and F. L. Martin, *Nat Protoc* **2016**, *11*, 664.
[18] C. L. M. Morais, K. M. G. Lima, M. Singh and F. L. Martin, *Nat Protoc* **2020**, *15*, 2143.
[19] Z. M. Zhang, S. Chen and Y. Z. Liang, *Analyst* **2010**, *135*, 1138.
[20] J. Team in *JASP (Version 0.14.1)*, *Vol.* **2020**.
[21] U. A. Walker, S. Collins and E. Byrne, *Eur Neurol* **1996**, *36*, 260.
[22] R. Al-Rifai, C. Tournois, S. Kheirallah, N. Bouland, G. Poitevin, P. Nguyen and A. Beljebbar, *Analyst* **2019**, *144*, 4677.
[23] N. Huang, M. Short, J. Zhao, H. Wang, H. Lui, M. Korbelik and H. Zeng, *Opt Express* **2011**, *19*, 22892.
[24] T. Minamikawa, Y. Harada and T. Takamatsu, *Sci Rep* **2015**, *5*, 17165.
[25] E. B. Carew, I. M. Asher and H. E. Stanley, *Science* **1975**, *188*, 933.
[26] Z. Huang, S. K. Teh, W. Zheng, K. Lin, K. Y. Ho, M. Teh and K. G. Yeoh, *Biosens Bioelectron* **2010**, *26*, 383.
[27] R. M. Spiers, J. Marzi, E. M. Brauchle, S. E. Cross, R. H. Vaughan, P. A. Bateman, S. J. Hughes, K. Schenke-Layland and P. R. V. Johnson, *Acta Biomater* **2019**, *99*, 269.
[28] I. Notingher, S. Verrier, S. Haque, J. M. Polak and L. L. Hench, *Biopolymers* **2003**, *72*, 230.
[29] W. A. Alaynick, *Mitochondrion* **2008**, *8*, 329.
[30] M. A. Johnson, J. Polgar, D. Weightman and D. Appleton, *J Neurol Sci* **1973**, *18*, 111.
[31] M. A. Johnson, G. Sideri, D. Weightman and D. Appleton, *J Neurol Sci* **1973**, *20*, 345.

[32] T. Kirchberger-Tolstik, O. Ryabchykov, T. Bocklitz, O. Dirsch, U. Settmacher, J. Popp and A. Stallmach, *Analyst* **2020**.
[33] L. M. Almond, J. Hutchings, G. Lloyd, H. Barr, N. Shepherd, J. Day, O. Stevens, S. Sanders, M. Wadley, N. Stone and C. Kendall, *Gastrointest Endosc* **2014**, *79*, 37.
[34] J. Langer, D. Jimenez de Aberasturi, J. Aizpurua, R. A. Alvarez-Puebla, B. Auguie, J. J. Baumberg, G. C. Bazan, S. E. J. Bell, A. Boisen, A. G. Brolo, J. Choo, D. Cialla-May, V. Deckert, L. Fabris, K. Faulds, F. J. Garcia de Abajo, R. Goodacre, D. Graham, A. J. Haes, C. L. Haynes, C. Huck, T. Itoh, M. Kall, J. Kneipp, N. A. Kotov, H. Kuang, E. C. Le Ru, H. K. Lee, J. F. Li, X. Y. Ling, S. A. Maier, T. Mayerhofer, M. Moskovits, K. Murakoshi, J. M. Nam, S. Nie, Y. Ozaki, I. Pastoriza-Santos, J. Perez-Juste, J. Popp, A. Pucci, S. Reich, B. Ren, G. C. Schatz, T. Shegai, S. Schlucker, L. L. Tay, K. G. Thomas, Z. Q. Tian, R. P. Van Duyne, T. Vo-Dinh, Y. Wang, K. A. Willets, C. Xu, H. Xu, Y. Xu, Y. S. Yamamoto, B. Zhao and L. M. Liz-Marzan, *ACS Nano* **2020**, *14*, 28.
[35] R. R. Jones, D. C. Hooper, L. Zhang, D. Wolverson and V. K. Valev, *Nanoscale Res Lett* **2019**, *14*, 231.

Variables	Mitochondrial disease (n=15)	Healthy Volunteers (n=10)	P value (statistical test)
Sex			
Gender Split (male: female)	9:6	6:4	P>0.9 (Fishers exact)
Age			
Mean (yrs)	49	33	P=0.02 (t-test)
Range (yrs)	25-80	17-54	
Muscle			
Biceps	-		
Quadriceps	3	-	
Tibialis Anterior	11	-	
Gracilis/Semitendinous	-	10	
Deltoid	1	-	
Specific Diagnoses (n)			
M.3243A>G	11	-	
POLG-related	3	-	
Single mtDNA deletion	1	-	

Table 1. Demographic and clinical characteristics.

The pathogenic m.3243A>G mutation is associated with several clinical syndromes, see Supplemental Table 1 for further information on the clinical features of patients in this cohort. POLG-related refers to recessive mutations in the gene encoding the catalytic subunit of

mitochondrial DNA polymerase gamma (POLG), required for faithful mtDNA replication. mtDNA = mitochondrial DNA.

	Sensitivity	*Specificity*	*Accuracy*	*AUROC*
PROBE				
PCA-LDA	81.6%	82.5%	82.0%	0.82
PLS-DA	72.5%	86.8%	79.5%	0.80
MICROSCOPE				
PCA-LDA	85.3%	80%	82.3%	0.85
PLS-DA	70.7%	85.7%	77.6%	0.79

Table 2. Classification performance between healthy volunteers and mitochondrial disease patients for different multivariate technique and the two equipment types.

Figure legends

Figure 1. Raman spectra in healthy muscle tissue and mitochondrial disease.

a: Fibre optic average Raman spectra (±s.d. shaded) obtained from healthy volunteer muscle samples (black) and those from patients with mitochondrial disease (red).

b: Fibre optic probe Mitochondrial disease – heathy volunteer subtraction spectra.

c: Microscope average Raman spectra (±s.d. shaded) obtained from healthy volunteer muscle samples (black) and those from patients with mitochondrial disease (red).

d: Microscope Mitochondrial disease – heathy volunteer subtraction spectra.

Figure 2. Difference spectra between different mitochondrial disease muscles healthy tissue.

a-d: Difference spectra for mitochondrial disease muscles and healthy muscle are similar for both the fibre optic probe (a & b) and microscope (c & d). This suggests that prominent features relate to the disease state, rather than differences between muscles.

e : Fibre optic probe difference spectra between quadriceps and tibialis anterior in the mitochondrial disease group. The resulting spectrum manifests different features to those observed between mitochondrial disease patients and healthy volunteers (see a-d).

f: Microscope difference spectra between quadriceps and tibialis anterior in the mitochondrial disease group. The spectrum consists of largely uninformative background (microscope, f).

Figure 3. LDF scores and plots for the fibre optic probe and microscope.

a-b. Fibre optic probe LDF scores and associated loadings plot. A significant difference in LDF scores was observed between the two groups.

c-d. Microscope LDF scores and associated loadings plot. A significant difference in LDF scores was observed between the two groups.

Figure 4. Detection of mitochondrial disease-related pathology.

a: PCA plots and performance statistics for three group models indicating detection of samples with reduced COX activity with the fibre optic probe.

b: PCA plots and performance statistics for three group models indicating detection of samples with diminished COX activity with the microscope.

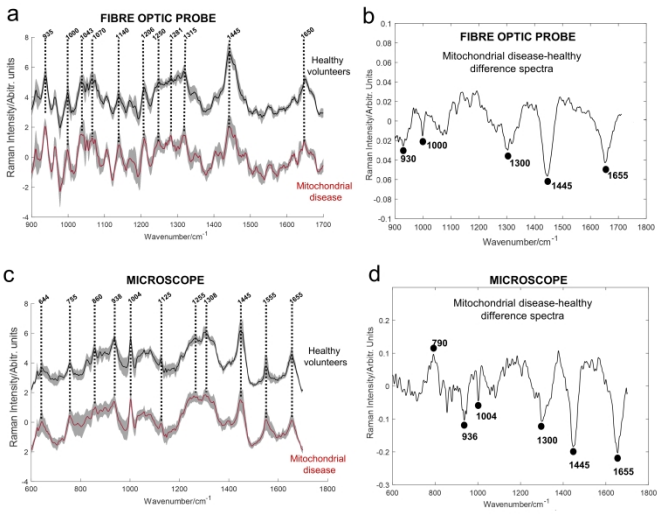

195x100mm (800 x 800 DPI)

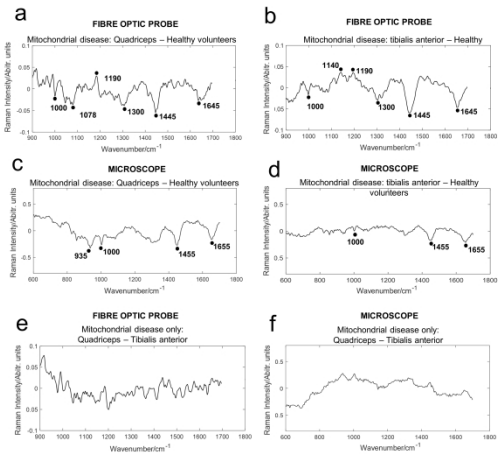

195x100mm (800 x 800 DPI)

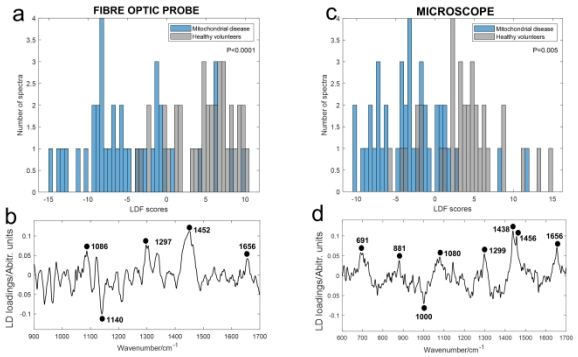

195x100mm (800 x 800 DPI)

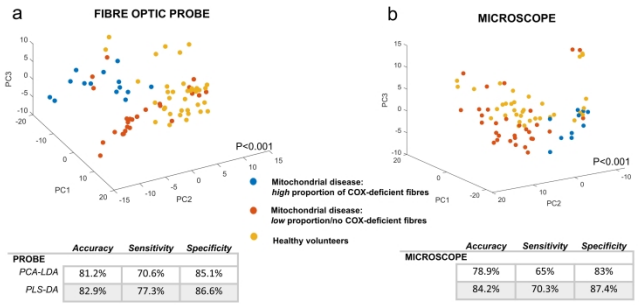

PROBE	Accuracy	Sensitivity	Specificity
PCA-LDA	81.2%	70.6%	85.1%
PLS-DA	82.9%	77.3%	86.6%

MICROSCOPE	Accuracy	Sensitivity	Specificity
	78.9%	65%	83%
	84.2%	70.3%	87.4%

195x100mm (800 x 800 DPI)

Gender	Muscle	Biopsy findings	Age	Genotype	Clinical phenotype	Muscle heteroplasmy (%)
F	TA	3% COX-deficient fibres, 1% ragged-red fibres	62y	m.3243A>G	Maternally inherited diabetes and deafness	38
F	VL	<1% COX-deficient fibres	29y	m.3243A>G	Mitochondrial encephalopathy, lactic acidosis, and stroke-like episodes	50
M	VL	4% COX-deficient fibres, 2% ragged-red fibres	31y	m.3243A>G	Asymptomatic	63
F	TA	4% COX-deficient fibres, 2% ragged-red fibres	53y	m.3243A>G	Maternally inherited diabetes and deafness	73
F	TA	1% COX-deficient fibres	55y	m.3243A>G	Maternally inherited diabetes and deafness, Left ventricular hypertrophy, GI dysmotility, Mild ataxia	84
M	TA	4% COX-deficient fibres, 2% ragged-red fibres	49y	m.3243A>G	Maternally inherited diabetes and deafness	74
M	VL	1% COX-deficient fibres	44y	m.3243A>G	Subtle progressive external ophthalmoplegia, myopathy, exercise intolerance SNHL	68

					Glucose intolerance	
M	TA	40% COX-deficient fibres, 20% ragged-red fibres	29y	Single, large-scale mtDNA deletion	Progressive external ophthalmoplegia, ptosis, exercise intolerance	Not determined
M	TA	normal	25y	m.3243A>G	Sensorineural hearing loss, short stature, Wolff-Parkinson-White syndrome	76
F	TA	1% COX-deficient fibres	45y	m.3243A>G	Maternally inherited diabetes and deafness	37
M	TA	25% COX-deficient fibres, 10% ragged-red fibres	54y	m.3243A>G	Mitochondrial encephalopathy, lactic acidosis, and stroke-like episodes	64
M	TA	30% COX-deficient fibres, 8% ragged-red fibres	58y	m.8344A>G	Myoclonic epilepsy with ragged red fibres. Patient 6 in[1]	90
M	TA	20% COX-deficient fibres, 5% ragged-red fibres	80y	Recessive *POLG* variants (p.Ala467Thr; p.Thr251Ile/p.Pro587Leu)	Progressive external ophthalmoplegia, ptosis, generalised myopathy. Patient 10 in[2]	N/A
M	TA	17% COX-deficient fibres, 8% ragged-red fibres	56y	Recessive *POLG* variants (p.Trp748Ser; p.Arg1096Cys)	Progressive external ophthalmoplegia, ptosis, peripheral neuropathy, epilepsy. Patient 5 in[3]	N/A
F	Delt	15% COX-deficient fibres, 4% ragged-red fibres	64y	Recessive *POLG* variants c.2542G>A p.(Gly848Ser);	Ptosis, peripheral neuropathy, ataxia	N/A

				c.2799T>G p.(Ser933Arg)		

Supplementary table 1. Clinico-pathological characteristics of the patients. References document previous reports that those patients have contributed to. M – male; F – female. TA – tibialis anterior, Delt – deltoid; COX – cytochrome c oxidase; y – years; N/A – not applicable.

Waven. (cm^{-1})	Assignment + references	Probe av.	M'scope av.	Probe subtn	M'scope subtn	Probe LDF	M'scope LDF
644	Tyrosine[4]		✓				
691	Lipid, methionine[5]						✓
755-60	Tryptophan[6]		✓				
790	DNA, Uracil[7]				✓		
860	Phosphate group[8]		✓				
881	Tryptophan[9]						✓
930-8	Proline, valine, protein backbone (α-helix)[10]	✓	✓		✓		
1000/4	Phenylalanine[7a, 10a, 11]	✓	✓	✓	✓		✓
1043	Proline[12]	✓					
1070	Lipids[13]	✓					
1075-86	Lipids[6, 14]			✓		✓	✓
1125	Valine[7a]		✓				
1140	Collagen[15]	✓				✓	
1190	Proline, valine[7a]			✓			
1206	Hydroxyproline (collagen)[6, 12]	✓					
1250-55	Amide III[11-12, 16]	✓	✓				
1280-1310	Amide III (α-helix)[10b, 17]	✓	✓	✓	✓		✓

1315	Guanine[18]	✓				✓	
1438	CH_2 deformation protein[19]						✓
1445-55	Collagen, lipids[14]	✓	✓	✓	✓	✓	✓
1550-55	Tryptophan, proteins		✓				✓
1645-60	Amide I (α-helix), Lipids[6, 12, 20]	✓	✓	✓	✓	✓	✓

Supplementary table 2. Tentative peak assignments. Abbreviations: M'scope = Microscope, av. = average, subtn = subtraction, LDF = linear discriminant function.

Figure legends

Supplementary figure 1.

Schematic of the fibre optic Raman probe and picture of the probe next to a muscle sample on a calcium fluoride slide.

Supplementary figure 2. Correlation of Raman spectra with age across all participants.

Partial least squares regression plots and statistics for the fibre optic probe and microscope. Leave-one-patient out cross validation was used. RMSECV – root mean square error of cross validation; CV = cross validation.

Supplemental figure 3. Microscope data with windowing from 900-1700 cm^{-1}.

a). Average Raman spectra (±s.d.) obtained from healthy volunteer muscle samples (black) and those from patients with mitochondrial disease (red).

b). Mitochondrial disease – heathy volunteer subtraction spectra.

c). LDF scores.

d). Associated LDF loadings plot.

Supplementary references

[1] N. Z. Lax, J. Grady, A. Laude, F. Chan, P. D. Hepplewhite, G. Gorman, R. G. Whittaker, Y. Ng, M. O. Cunningham and D. M. Turnbull, *Neuropathol Appl Neurobiol* **2016**, *42*, 180-193.
[2] A. Chrysostomou, J. P. Grady, A. Laude, R. W. Taylor, D. M. Turnbull and N. Z. Lax, *Neuropathol Appl Neurobiol* **2016**, *42*, 477-492.
[3] N. Z. Lax, R. G. Whittaker, P. D. Hepplewhite, A. K. Reeve, E. L. Blakely, E. Jaros, P. G. Ince, R. W. Taylor, P. R. Fawcett and D. M. Turnbull, *Brain* **2012**, *135*, 62-71.
[4] S. Koljenovic, T. C. Bakker Schut, J. P. van Meerbeeck, A. P. Maat, S. A. Burgers, P. E. Zondervan, J. M. Kros and G. J. Puppels, *J Biomed Opt* **2004**, *9*, 1187-1197.
[5] A. Momenpour, P. D. A. Lima, Y. A. Chen, C. R. Tzeng, B. K. Tsang and H. Anis, *Biomed Opt Express* **2018**, *9*, 801-817.
[6] N. Stone, C. Kendall, J. Smith, P. Crow and H. Barr, *Faraday Discuss* **2004**, *126*, 141-157; discussion 169-183.
[7] a) J. De Gelder, K. De Gussem, P. Vandenabeele and L. Moens, *Journal of Raman Spectroscopy* **2007**, *38*, 1133-1147; b) A. Azan, V. Untereiner, C. Gobinet, G. D. Sockalingum, M. Breton, O. Piot and L. M. Mir, *Scientific Reports* **2017**, *7*, 40448.
[8] C. Krafft, L. Neudert, T. Simat and R. Salzer, *Spectrochim Acta A Mol Biomol Spectrosc* **2005**, *61*, 1529-1535.
[9] G. Shetty, C. Kendall, N. Shepherd, N. Stone and H. Barr, *Br J Cancer* **2006**, *94*, 1460-1464.
[10] a) N. Stone, C. Kendall, N. Shepherd, P. Crow and H. Barr, *Journal of Raman Spectroscopy* **2002**, *33*, 564-573; b) M. Pezolet, M. Pigeon-Gosselin, J. Nadeau and J. P. Caille, *Biophys J* **1980**, *31*, 1-8.
[11] G. Zhu, X. Zhu, Q. Fan and X. Wan, *Spectrochim Acta A Mol Biomol Spectrosc* **2011**, *78*, 1187-1195.
[12] C. J. Frank, R. L. McCreery and D. C. Redd, *Anal Chem* **1995**, *67*, 777-783.
[13] L. Silveira, Jr., S. Sathaiah, R. A. Zangaro, M. T. Pacheco, M. C. Chavantes and C. A. Pasqualucci, *Lasers Surg Med* **2002**, *30*, 290-297.
[14] Z. Huang, A. McWilliams, H. Lui, D. I. McLean, S. Lam and H. Zeng, *Int J Cancer* **2003**, *107*, 1047-1052.
[15] C. Yorucu, K. Lau, S. Mittar, N. H. Green, A. Raza, I. U. Rehman and S. MacNeil, *Appl Spectrosc Rev* **2016**, *51*, 243-257.
[16] M. Gniadecka, H. C. Wulf, N. Nymark Mortensen, O. Faurskov Nielsen and D. H. Christensen, *Journal of Raman Spectroscopy* **1997**, *28*, 125-129.
[17] a) M. Pezolet, M. Pigeon, D. Menard and J. P. Caille, *Biophys J* **1988**, *53*, 319-325; b) H. Sato, Y. Maeda, M. Ishigaki and B. Andriana in *Biomedical Applications of Raman Spectroscopy*, (Ed. R. A. Meyers), **2014**, pp. 1-12.
[18] A. Mahadevan-Jansen, M. F. Mitchell, N. Ramanujam, A. Malpica, S. Thomsen, U. Utzinger and R. Richards-Kortum, *Photochem Photobiol* **1998**, *68*, 123-132.
[19] a) N. Amharref, A. Beljebbar, S. Dukic, L. Venteo, L. Schneider, M. Pluot and M. Manfait, *Biochim Biophys Acta* **2007**, *1768*, 2605-2615; b) Q. Zheng, J. Li, L. Yang, B. Zheng, J. Wang, N. Lv, J. Luo, F. L. Martin, D. Liu and J. He, *Analyst* **2020**, *145*, 385-392.
[20] R. Jyothi Lakshmi, V. B. Kartha, C. Murali Krishna, R. S. JG, G. Ullas and P. Uma Devi, *Radiat Res* **2002**, *157*, 175-182.

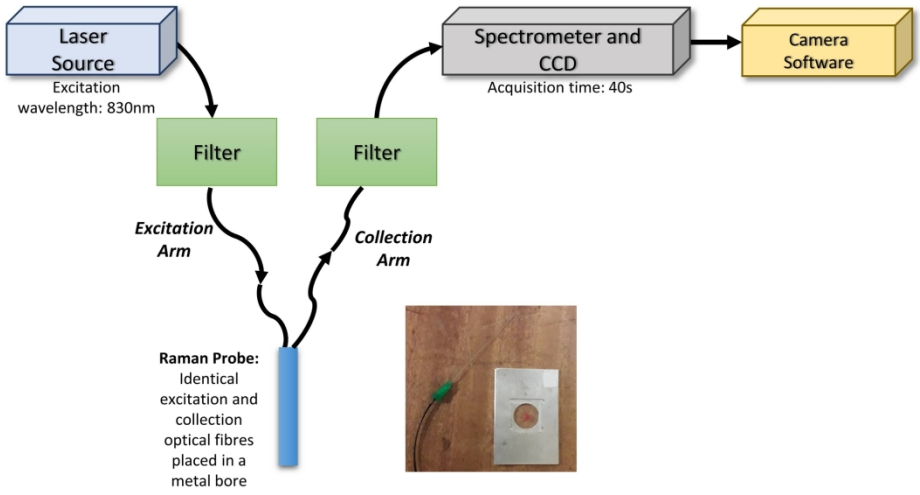

194x99mm (300 x 300 DPI)

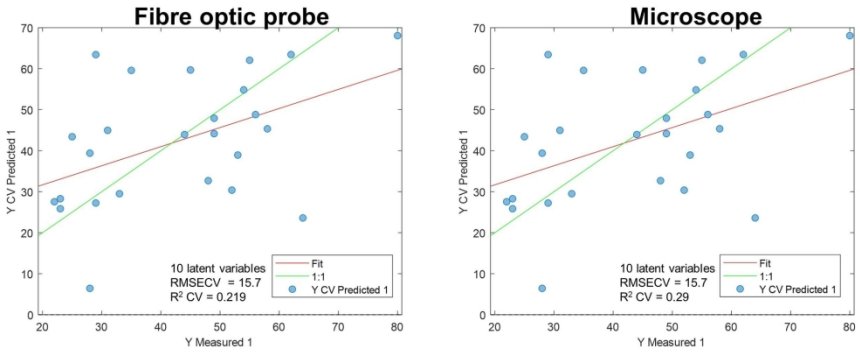

93x45mm (600 x 600 DPI)

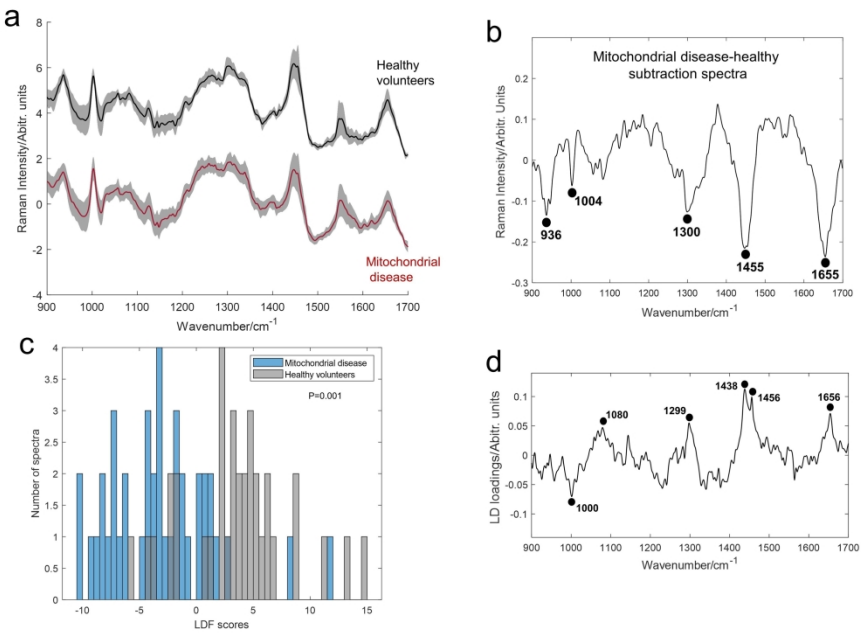

145x96mm (600 x 600 DPI)

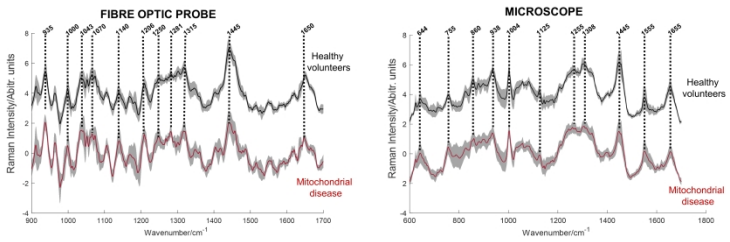

Mitochondrial diseases are devastating conditions that can be difficult to diagnose. This paper explores the potential of two different formats of Raman spectroscopy to identify mitochondrial disease from human muscle samples: a miniaturised fibre optic Raman system and a standard commercial Raman microscope. Both formats demonstrated high levels of disease classification accuracy (~80%). Raman spectroscopy of muscle may be a useful technique for the rapid identification of mitochondrial disease.

195x100mm (800 x 800 DPI)